Second-forbidden nonunique β^- decays of ^{59,60}Fe: Possible candidates for $g_{\rm A}$ sensitive electron spectral-shape measurements

Anil Kumar[1*], Praveen C. Srivastava[1†] and Jouni Suhonen[2‡]
[1] *Department of Physics, Indian Institute of Technology Roorkee, Roorkee 247667, India and*
[2] *University of Jyvaskyla, Department of Physics, P.O. Box 35 (YFL), FI-40014, University of Jyvaskyla, Finland*

(Dated: June 30, 2021)

In this work, we present a theoretical study of the electron spectral shapes for the second-forbidden nonunique β^--decay transitions ^{59}Fe$(3/2^-) \to {}^{59}$Co$(7/2^-)$ and ^{60}Fe$(0^+) \to {}^{60}$Co(2^+) in the framework of the nuclear shell model. We have computed the involved wave functions by carrying out a complete $0\hbar\omega$ calculation in the full fp model space using the KB3G and GXPF1A effective interactions. When compared with the available data, these interactions predict the low-energy spectra and electromagnetic properties of the involved nuclei quite successfully. This success paves the way for the computations of the β-decay properties, and comparison with the available data. We have computed the electron spectral shapes of the mentioned decay transitions as functions of the value of the weak axial coupling $g_{\rm A}$. By comparing these computed shapes with the measured spectral shapes allows then to extract the effective value of $g_{\rm A}$ for these decay transitions. This procedure, coined the spectrum-shape method (SSM) in several earlier studies, complements the method of determining the value of $g_{\rm A}$ by reproducing the (partial) half-lives of decay transitions. Here we have enhanced the original SSM by constraining the value of the relativistic vector matrix element, ${}^V\mathcal{M}^{(0)}_{KK-11}$, using the conserved vector-current hypothesis (CVC) as a starting point. We hope that this finding would be a strong incentive to measure the spectral shapes in the future.

PACS numbers: 21.60.Cs - shell model, 23.40.-s -β-decay

I. INTRODUCTION

The nuclear β decay can be considered as a mutual interaction between the hadronic and leptonic current mediated by a massive $W^\pm$ vector bosons. These currents can be expressed as mixtures of the vector and axial-vector contributions. The values of the weak coupling constants enter the theory of β-decay when the hadronic current is renormalized at the nucleon level [1]. The free-nucleon value of the vector coupling $g_{\rm V} = 1.00$ and axial-vector coupling $g_{\rm A} = 1.27$ derive from the conserved vector-current (CVC) hypothesis and the partially conserved axial-vector-current (PCAC) hypothesis, respectively [2]. The value of $g_{\rm A}$ is affected inside nuclear matter by nuclear many-body, delta-nucleon and mesonic correlations. The effect of these corrections on the bare value of $g_{\rm A}$ can be represented as an effective value $g_{\rm A}^{\rm eff} = qg_{\rm A}$, where q is a quenching factor. The effective value of $g_{\rm A}$ plays an important role when data on astrophysical processes, single beta decays and double beta decays are to be reproduced by nuclear many-body calculations. In the single β decays, the decay rate depends on the second power of $g_{\rm A}$, while to the forth power for $\beta\beta$ decays [3, 4]. A comprehensive review of the $g_{\rm A}$ problem in β and $\beta\beta$ decays is reported in Ref. [5]. A recent review of the theoretical and experimental status for the single and double β decay is given in [6].

Different methods have been used to extract information on the effective value of $g_{\rm A}$. One possibility is the half-life method where the computed and experimental (partial) β-decay half-lives are matched by varying the value of $g_{\rm A}$. This method has been used for the allowed, forbidden, and two-neutrino double β decays in the framework of the proton-neutron quasiparticle random-phase approximation (pnQRPA) [7–14], the nuclear shell model (NSM) [15–22], and the interacting boson model (IBM) [23–25]. All these studies have shown that a quenched value of $g_{\rm A}$ is needed in order to reproduced the experimental observations.

At this point it is worth pointing out that in the present and the above-referenced works an important component of nuclear structure has been omitted. This component are the two-body (meson-exchange) currents which go beyond the usually adopted impulse approximation of the weak nuclear decays. These currents have long been known to be active in the first-forbidden non-unique pseudoscalar $0^- \leftrightarrow 0^+$ beta-decay transitions governed by the relativistic axial rank-0 matrix element. For these transitions an enhancement, instead of quenching, has been recorded (see, e.g., [5, 26–28]). The two-body currents are also active in the allowed Gamow-Teller transitions, and taking them into account reduces drastically the need for the $g_{\rm A}$ quenching, as demonstrated for the very light nuclei in [29, 30] and light nuclei and light medium-mass nuclei in [31]. The studies reproduce well beta-decay rates using an unquenched value of $g_{\rm A}$ by means of including additional nuclear correlations and the two-body currents, as discussed in the review [32].

Regarding the role of many-body correlations and the

*akumar5@ph.iitr.ac.in
†Corresponding author: praveen.srivastava@ph.iitr.ac.in
‡jouni.t.suhonen@jyu.fi

choice of model space, the treatment of Gamow-Teller transitions and forbidden transitions may need a different degree of sophistication. In particular, for the Gamow-Teller transitions a $0\hbar\omega$ calculation, within one single oscillator major shell, is a good approximation, but for the second-forbidden beta transitions, discussed in the present work, the situation is not that clear. For the second-forbidden transitions the transition operators tend to pick $2\hbar\omega$ contributions neglected in the present calculations. As discussed below, this is reflected in the value of a key relativistic vector matrix element, which in our calculations vanishes, but should have a non-zero value according to the CVC hypothesis. The evidence from the electric quadrupole ($E2$) transitions is that the $2\hbar\omega$ contributions can be accounted for by the use of effective charges that in the standard form enhance the isoscalar contribution without modifying the isovector one, which is relevant for beta decay. However, there are no estimates about the role of the $2\hbar\omega$ correlations in the context of spin-quadrupole transitions, mediated by the axial second-forbidden operators relevant for the present calculations.

In Ref. [33], for the first time, another method to determine the effective value of $g_{\rm A}$, coined the spectrum-shape method (SSM), was introduced. In the SSM, an electron spectral shape is computed as a function of the value of $g_{\rm A}$, and then compared with the corresponding experimental shape, in order to find the effective $g_{\rm A}$ for which the computed spectral shape matches the experimental one. This method is applicable to forbidden nonunique β decays since the associated electron spectra depend on the details of nuclear structure. In Ref [33] also the next-to-leading-order (NLO) corrections were included in the spectral shape.

In Ref. [33] the shape of the electron spectrum for the forth-forbidden nonunique β^- decay of ^{113}Cd was computed under the framework of the microscopic quasiparticle-phonon model (MQPM) and the NSM. This work was extended in Ref. [34] to include a comparison with the results of the third nuclear model, IBM. In [34] the computed spectral shapes were compared with the measured one of Belli et al. [35], and the closest match was found for the ratio of $g_{\rm A}/g_{\rm V} \approx 0.92$ for all three nuclear models.

In continuation, electron spectral shapes for several experimentally interesting odd-A nuclei (MQPM and NSM calculations) and even-A nuclei (NSM calculations) were studied for their $g_{\rm A}$ dependence in Refs. [36, 37]. In Refs. [33, 36, 37] it was found that the spectral shapes for the β decays of ^{87}Rb, ^{94}Nb, ^{98}Tc, ^{99}Tc, ^{113}Cd, and ^{115}In depend strongly on the effective value of $g_{\rm A}$, thus rendering these decays as excellent candidates for applications of the SSM.

Recently, in Ref. [38] the electron spectral shapes of the second-forbidden nonunique β^- decays of ^{24}Na and ^{36}Cl were studied. It was found that the potential of the SSM could be enhanced by constraining the magnitude of the small relativistic vector matrix element, ${}^{V}\mathcal{M}^{(0)}_{211}$, by the measured decay half-life. This then leads to a consistent treatment of both the half-life and the spectral shape. Another approach, using the CVC to constrain the value of ${}^{V}\mathcal{M}^{(0)}_{211}$, was used for the second-forbidden nonunique β^- decay of ^{20}F in [39, 40].

In order to extend the SSM studies, we have tried to find new candidates for the application of the SSM by scanning through the fp shell and doing spectral-shape calculations using well established shell-model Hamiltonians. In this region of the nuclear chart we have found two possible candidate transitions, $^{59}\mathrm{Fe}(3/2^-) \rightarrow {}^{59}\mathrm{Co}(7/2^-)$ and $^{60}\mathrm{Fe}(0^+) \rightarrow {}^{60}\mathrm{Co}(2^+)$, which correspond to second-forbidden nonunique β^- decays with a Q values of 1.565 MeV and 0.178 MeV, branching ratios of 0.18(4)% and 100%, and partial half-lives of 67.72 years and 2.62×10^6 years, respectively. Here we study these transitions by carrying out complete $0\hbar\omega$ shell-model calculations in a full fp model space by using the well-established two-body interactions GXPF1A [41, 42] and KB3G [43]. Here it is worth mentioning that results for the ^{59}Fe electron spectra, corresponding to the GXPF1A interaction, have previously been reported in Ref. [26]. However, there the calculations were done in a very restricted model space and the drawn conclusion about the sensitivity to the SSM analysis differs from the conclusions of the present calculations.

In the present work, we enhance the original SSM in two different ways: either by i) constraining the value of the relativistic vector matrix element, ${}^{V}\mathcal{M}^{(0)}_{KK-11}$, using the CVC as described in [44], or ii) using the value of the matrix element as a fit parameter to reproduce the partial half-life of the decay transition. The former method requires an "ideal" nuclear-structure calculation, but in the present calculations we have to confine ourselves to the impulse approximation and a finite single-particle space, making the method i) only approximative in the present case. Nevertheless, the results of method i) can serve as rough estimates of the order of magnitude and sign of ${}^{V}\mathcal{M}^{(0)}_{KK-11}$, thus giving the method ii) a good starting point for the half-life fit. By using these two methods, we want to test how sensitively the prediction for the spectral shape depends on the method used to obtain it.

In order to test the predictive power of our computed nuclear wave functions, we have calculated the energy spectra for low-lying states as well as other spectroscopic properties of both the parent and daughter nuclei involved in the studied β-decay transitions. All these computed quantities turn out to be in good agreement with the available data. After all these comparisons we finally compute the electron spectral shapes as functions of the value of $g_{\rm A}$. It turns out that the spectral shapes obtained by using the method ii) dependent rather sensitively on the value of $g_{\rm A}$. Since in the case of the present, non-ideal, calculations the method ii) is to be viewed as more reliable, the enhanced SSM can be considered as a powerful probe for the studied transitions. We hope that these findings serve as a strong incentive to measure the involved spectral shapes in the future.

The current article is organized as follows. In Sec. II we give a short overview of the adopted theoretical formalism for β-decay. Results and discussions are reported in Sec. III and, finally, in Sec. IV, we conclude.

II. THEORETICAL FORMALISM

In Sec. II A, we discuss the theory of forbidden nonunique β^- decays, and the shape of the electron spectra. In Sec. II B we give the details about the valence space and effective Hamiltonian used in the present work.

A. β-decay theory

In the literature, the theoretical framework of the β decay is well established in the book by Behrens and Bühring [44] (see also Ref. [45]). We have used the streamlined version of the formalism for the forbidden nonunique β^--decay theory from Refs. [34, 46]. To simplify the β^--decay theory, we have used the impulse approximation, in which at the exact moment of the decay, only the decaying nucleon feels the weak interaction and the strong interactions with the remaining $A-1$ nucleons are ignored [47]. For the β^--decay process, described as an effective point-like interaction vertex with an effective coupling constant $G_{\rm F}$, called Fermi coupling constant, the probability of the emitted electron to have a kinetic energy between W_e and $W_e + dW_e$ is given by

$$P(W_e)dW_e = \frac{G_{\rm F}^2}{(\hbar c)^6}\frac{1}{2\pi^3\hbar}C(W_e)p_e c W_e(W_0 - W_e)^2 \times F_0(Z, W_e)dW_e, \quad (1)$$

where W_0 is the endpoint energy of the β spectrum, the factor $F_0(Z, W_e)$ is the Fermi function, and Z is the proton number of the daughter nucleus. The p_e and W_e are the momentum and energy of the emitted electron, respectively. Furthermore, the shape factor $C(W_e)$ contains the nuclear-structure information.

The partial half-life of the decay process can be written as

$$t_{1/2} = \frac{\ln(2)}{\int_{m_e c^2}^{W_0} P(W_e)dW_e} = \frac{\kappa}{\tilde{C}}, \quad (2)$$

where m_e is the rest mass of the electron, $\tilde{C}$ is the dimensionless integrated shape function, and the updated [48] value of constant κ is

$$\kappa = \frac{2\pi^3\hbar^7\ln(2)}{m_e^5 c^4 (G_{\rm F}{\rm Cos}\theta_{\rm C})^2} = 6289 \text{ s}, \quad (3)$$

where the $\theta_{\rm C}$ is the Cabibbo angle. To simplify the formalism it is usual to adopt the unitless scaled kinematics quantities $w_0 = W_0/m_e c^2$, $w_e = W_e/m_e c^2$, and $p = p_e c/m_e c^2 = \sqrt{(w_e^2 - 1)}$. Using the unitless quantities the dimensionless integrated shape function reads

$$\tilde{C} = \int_1^{w_0} C(w_e) p w_e (w_0 - w_e)^2 F_0(Z, w_e) dw_e. \quad (4)$$

The general form of the shape factor $C(w_e)$ can be expressed as

$$C(w_e) = \sum_{k_e, k_\nu, K} \lambda_{k_e}\Big[M_K(k_e, k_\nu)^2 + m_K(k_e, k_\nu)^2 - \frac{2\gamma_{k_e}}{k_e w_e} M_K(k_e, k_\nu) m_K(k_e, k_\nu)\Big], \quad (5)$$

where the k_e and k_ν (both are running through 1, 2, 3,...) are the positive integers emerging from the partial-wave expansion of the leptonic wave functions, and K is the order of the forbiddenness. The quantities $M_K(k_e, k_\nu)$ and $m_K(k_e, k_\nu)$ contain all the nuclear-structure information in the form of different nuclear matrix elements (NMEs) and leptonic phase-space factors. More information on these expressions can be found in Ref. [44] (also given in Ref. [34]). Here $\gamma_{k_e} = \sqrt{k_e^2 - (\alpha Z)^2}$ and the quantity $\lambda_{k_e} = F_{k_e - 1}(Z, w_e)/F_0(Z, w_e)$ is the Coulomb function, where $F_{k_e-1}(Z, w_e)$ is the generalized Fermi function [34, 46].

The NMEs contains all the nuclear-structure information in the form

$$^{V/A}\mathcal{M}^{(N)}_{KLS}(pn)(k_e, m, n, \rho) = \frac{\sqrt{4\pi}}{\widehat{J}_i}\sum_{pn} {}^{V/A}m^{(N)}_{KLS}(pn)(k_e, m, n, \rho)(\Psi_f||[c_p^\dagger \tilde{c}_n]_K||\Psi_i), \quad (6)$$

where the quantities $^{V/A}m^{(N)}_{KLS}(pn)(k_e, m, n, \rho)$ are called the single-particle matrix elements (SPMEs), which characterize the properties of the transition operators, and they are the same for all the nuclear models. In our calculations, the SPMEs are computed in basis of harmonic-oscillator wave functions [34, 46]. The quantities $(\Psi_f||[c_p^\dagger \tilde{c}_n]_K||\Psi_i)$ are the one-body transition densities (OBTDs) between the initial (Ψ_i) and final (Ψ_f) states. The OBTDs contain the nuclear-structure information and they must be evaluated separately for each nuclear model. The summation runs over the proton (p) and neutron (n) single-particle states and the "hat-notation" reads $\widehat{J}_i = \sqrt{2J_i + 1}$. The Coulomb-corrected NMEs are indicated by the notation (k_e, m, n, ρ) when such matrix elements exist, and they are characterized by using the integers m, n, and ρ, where the order m is the total power of the factors $(m_e R)$, $(W_e R)$ and (αZ), the number n is the total power of the factors $(W_e R)$ and (αZ) and the number ρ the power of the factor (αZ). Here R is the nuclear radius, and L and S are the total orbital angular momentum and spin of the leptons,

respectively. The label N refers to the power of the qR when expanding the form factors, where q is the momentum transfer.

The shape factor depends on the weak coupling constants $g_{\rm V}$ and $g_{\rm A}$. So the shape factor can be decomposed into vector, axial-vector and mixed vector-axial-vector components [33, 34, 36, 37] based on the weak coupling constants they contain. In this spirit we can write

$$C(w_e) = g_{\rm V}^2 C_{\rm V}(w_e) + g_{\rm A}^2 C_{\rm A}(w_e) + g_{\rm V} g_{\rm A} C_{\rm VA}(w_e). \quad (7)$$

After integrating Eq. (7) with respect to electron kinetic energy, we obtain a decomposition of the dimensionless integrated shape function (4) in the form.

$$\tilde{C} = g_{\rm V}^2 \tilde{C}_{\rm V} + g_{\rm A}^2 \tilde{C}_{\rm A} + g_{\rm V} g_{\rm A} \tilde{C}_{\rm VA}. \quad (8)$$

The shape factors C_i in Eq. (7) depend on the electron kinetic energy, while after the integration the (partial) shape functions $\tilde{C}_i$ in Eq. (8) are just constant numbers.

B. Adopted model space and Hamiltonians

For the calculations of the OBTDs, needed for the evaluation of the NMEs contained in the β-decay amplitudes, we need to choose a nuclear model. In the present work, the wave functions of the initial and final states were computed by using the nuclear shell model (NSM). The shell-model wave functions and OBTDs were computed using the nuclear shell-model code NuShellX@MSU [49] with the well-known effective interactions KB3G and GXPF1A in the full fp model space. In the present studies, we have parformed complete $0\hbar\omega$ calculations in the full fp model space.

III. RESULTS AND DISCUSSIONS

In this section we present our computed results of low-lying energy spectra, spectroscopic properties, shape factors and electron spectra for the second-forbidden nonunique β^--decay transitions ^{59}Fe$(3/2^-) \rightarrow$ ^{59}Co$(7/2^-)$ and ^{60}Fe$(0^+) \rightarrow$ ^{60}Co(2^+).

The NSM-computed electron spectrum for the decay of ^{60}Fe is already available in Ref. [37], but in a heavily truncated model space. In the present work, we have performed complete $0\hbar\omega$ shell-model calculations in a full fp model space with recent well-established interactions. As in the works [26, 33, 34, 36, 37], we have included here the next-to-leading-order (NLO) corrections to the shape factor. In this way, the number of NMEs increases drastically, and in the case of the second-forbidden nonunique β^- decay, the number of NMEs is increased from 8 to 27 (see the full details about the NLO corrections in Refs. [33, 34]).

Below we present low-lying energy spectra (Figs. 1 and 2), spectroscopic properties (Table I and II), the computed NMEs (Tables III-V), electron spectral shapes as functions of the electron kinetic energy (Figs. 4-7), the NLO corrections in the half-life and electron spectra (Figs. 8 and 9), and decompositions of the integrated shape functions (Table VI).

A. Low-lying energy spectra and spectroscopic properties

We have performed shell-model calculations for the ground state and a few low-lying excited states of the β^--decay parent and daughter nuclei of the studied transitions by using the KB3G and GXPF1A interactions in a full fp model space, performing complete $0\hbar\omega$ shell-model calculations.

The computed energy spectra of low-lying states in ^{59}Fe and ^{59}Co are presented in Fig. 1 and compared with the available experimental data. As seen in Fig. 1, the computed ground states are correctly reproduced by the KB3G and GXPF1A interactions for ^{59}Fe and ^{59}Co. Also the computed excited states are in the right energy regions, though some inversions in the relative ordering of the states occur for both interactions. In Fig. 2, we show the low-energy spectra of ^{60}Fe and ^{60}Co and their comparison with the experimental data. As seen in Fig. 2, the computed first 2^+ state for ^{60}Fe is obtained at 0.788 and 0.817 MeV corresponding to the KB3G and GXPF1A interactions, respectively, while the experimental value is 0.823 MeV. For ^{60}Co, the KB3G and GXPF1A interactions give a 2^+ state as the ground state while the experimental ground state is 5^+. From the KB3G calculation, the first excited 5^+ state is obtained at 0.034 MeV while the GXPF1A calculation places it at 0.162 MeV. For both ^{60}Fe and ^{60}Co the computed spectra contain the spin-parities of the experimental spectra in roughly the right energy ranges, but sometimes in inverted orderings.

The computed results for quadrupole and magnetic moments are shown in Table I and compared with available experimental data. In most cases, both moments are well reproduced by both interactions. The computed $B(E2)$ values are presented in Table II. Our computed results of electromagnetic properties are in good agreement with the available experimental data. Present calculations also reproduce correctly the signs of the quadrupole and magnetic moments. Overall, the spectroscopic properties of the presently discussed fp-shell nuclei are fairly well reproduced by both the adopted effective interactions. This gives us confidence for a successful computation of the β-decay properties, discussed in the following section.

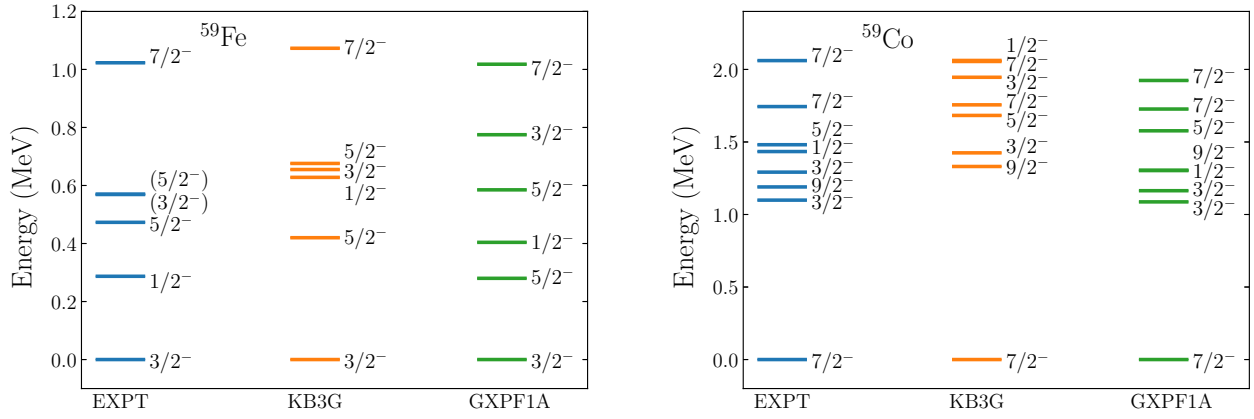

FIG. 1: Comparison of the KB3G- and GXPF1A-computed energy spectra with the experimental [50] one for the low-lying energy spectra of ^{59}Fe and ^{59}Co.

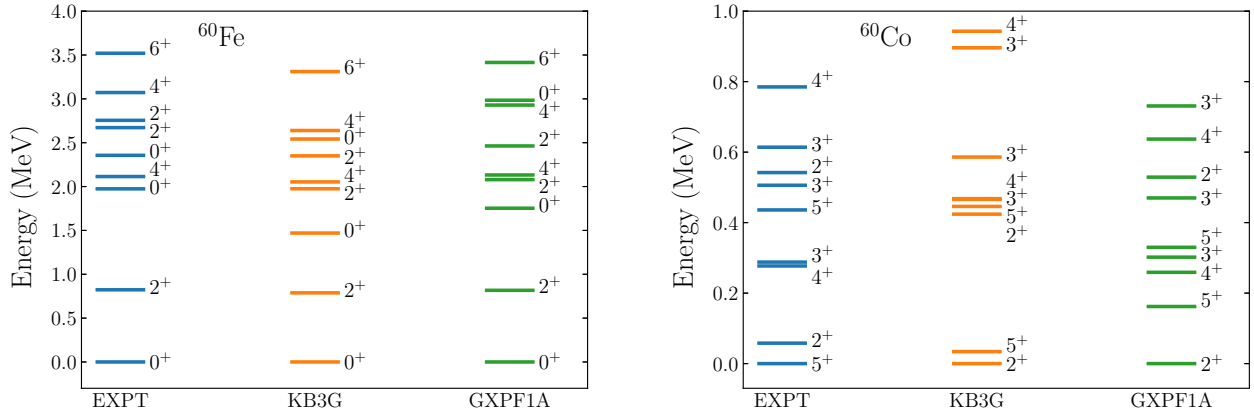

FIG. 2: Comparison of the KB3G- and GXPF1A-computed energy spectra with the experimental [50] one for the low-lying energy spectra of ^{60}Fe and ^{60}Co.

TABLE I: Comparison of the computed quadrupole and magnetic moments with available experimental data. For the calculations, we have used the effective charges $e_p = 1.5e$ and $e_n = 0.5e$, and bare g factors ($g^{\rm eff} = g^{\rm free}$). The experimental values are taken from [50].

		$Q(eb)$			$\mu(\mu_N)$		
		Expt.	KB3G	GXPF1A	Expt.	KB3G	GXPF1A
^{59}Fe	$3/2^-$	N/A	+0.21	+0.24	-0.3358 (4)	-0.24	-0.08
^{59}Co	$7/2^-$	+0.42 (3)	+0.38	+0.44	+4.627 (9)	+4.51	+4.59
^{60}Fe	2^+	N/A	-0.28	-0.30	N/A	+1.06	+1.11
^{60}Co	5^+	+0.44 (5)	+0.44	+0.51	+3.799 (8)	+3.66	+3.95
	2^+	+0.3 (4)	+0.23	+0.26	+4.40 (9)	+4.60	+4.26

B. Nuclear matrix elements

Once the shell-model description of low-energy spectra and spectroscopic properties of the involved nuclei is now under control, we are ready to use the resulting wave functions to compute the OBTDs needed in the NMEs for the β-decay-rate calculations.

The main theme of the present calculations is to vary

TABLE II: Comparison of the computed and experimental $B(E2)$ values in W.u. The effective charges $e_p = 1.5e$ and $e_n = 0.5e$ were used. The experimental values are taken from [50].

	Transitions	Expt.	KB3G	GXPF1A
^{59}Fe	$B(E2; 7/2^- \to 3/2^-)$	N/A	12.36	14.42
^{59}Co	$B(E2; 3/2^- \to 7/2^-)$	9.2 (20)	6.45	0.47
^{60}Fe	$B(E2; 2^+ \to 0^+)$	13.6 (14)	15.53	18.89
^{60}Co	$B(E2; 4^+ \to 2^+)$	N/A	0.69	0.57

the value of the axial coupling strength $g_{\rm A}$ and see how it affects the electron spectral shapes of the second-forbidden nonunique β^--decay transitions ^{59}Fe$(3/2^-) \to$ ^{59}Co$(7/2^-)$ and ^{60}Fe$(0^+) \to$ ^{60}Co(2^+). In order to (possibly) gain a rough idea about the possible values of this coupling in the presently discussed mass region, we have studied the decay rates of two measured allowed transitions in ^{59}Fe. In Table III, we present our calculated absolute values of the Gamow-Teller ($\mathcal{M}_{\rm GT}$) and Fermi ($\mathcal{M}_{\rm F}$) matrix elements for these allowed transitions from the $3/2^-$ ground state of ^{59}Fe to the first two $3/2^-$ excited states in ^{59}Co. The experimental $\mathcal{M}_{\rm GT}$ NMEs are obtained by using the experimental log ft values [50] and the information that the Fermi NMEs can be neglected based on our calculated numbers, presented in the table. Fermi matrix elements for the allowed transitions in ^{59}Fe are tiny due to isospin conservation. For the transition $3/2^- \to 3/2^-_1$, the KB3G-computed magnitude of $\mathcal{M}_{\rm GT}$ is found consistent with the experimental one, while for the GXPF1A interaction the computed value is far from the experimental one. In the case of the $3/2^- \to 3/2^-_2$ transition, our calculated absolute values of $\mathcal{M}_{\rm GT}$ for both interactions are far too small compared to the data. Unfortunately, our attempt, did not lead to any clarification of the $g_{\rm A}$ problem due to the vastly different predicted values of the Gamow-Teller matrix elements for the two interactions and two transitions. It seems that the prediction of the exact structure of the higher-lying excited states is not so trivial for the presently used shell-model interactions. Therefore, we have to perform our SSM analyses for the second-forbidden nonunique β^- decays of ^{59,60}Fe without any perception of a possible preferred effective value of $g_{\rm A}$.

The KB3G- and GXPF1A-computed NMEs for the second-forbidden nonunique β^- decays of ^{59,60}Fe are presented in Table IV. The relativistic vector NME $^V\mathcal{M}^{(0)}_{KK-11}$ becomes identically zero due to the limitation of our adopted single-particle model space (see more details in Refs. [38, 39]). For convenience of notation, we will call this NME as s-NME (small NME). As mentioned in the introduction, we constrain the value of this matrix element by two different ways: either i) from the CVC relation as described in [44], or ii) by reproducing the experimental partial half-life by tuning this matrix element separately for each value of $g_{\rm A}$. In the method i), the mentioned CVC relation [44] reads

$$^V F^{(0)}_{211} = -\frac{1}{\sqrt{10}}\left[W_0 R - (M_n - M_p)R + \frac{6}{5}\alpha Z\right] {}^V F^{(0)}_{220}, \tag{9}$$

where the $^V F^{(N)}_{KLS}$ are the form factor coefficient which are related to the NMEs via

$$R^{LV} F^{(N)}_{KLS}(k_e, m, n, \rho) = (-1)^{K-L} g_{\rm V} {}^V\mathcal{M}^{(N)}_{KLS}(k_e, m, n, \rho). \tag{10}$$

The values of the CVC-constrained small nuclear matrix element s-NME, obtained from the above relations using the computed values of the large vector NME $^V\mathcal{M}^{(0)}_{KK0}$, are presented in Table IV with the additional label "CVC". The large NME receives the bulk of its contributions from the presently used single-particle model space so that its value can be considered as quite reasonable. In the method ii), we have used the s-NME as a fit parameter to reproduce the measured partial half-life of the decay transition for each $g_{\rm A}$ separately, and the corresponding s-NME values are presented in Table V. In Table IV, the CVC-constrained s-NMEs are compared with the fit-parameter s-NMEs, obtained by using $g_{\rm A} = 0.80$. It can be seen that the fitted values of the s-NMEs are of the same order of magnitude as the CVC-constrained ones, differing by a factor $2-3$ from each other.

As seen in Tables IV and V, the leading-order (LO) s-NME, $^V\mathcal{M}^{(0)}_{KK-11}$, is roughly three orders of magnitude smaller than the LO large vector NME $^V\mathcal{M}^{(0)}_{KK0}$. However, owing to the systematic order-by-order expansion of Behrens and Bühring [44], their contributions to the $M_K(k_e, k_\nu)$ and $m_K(k_e, k_\nu)$ matrix elements of Eq. (5) are on equal footing. This is quaranteed by the smaller phase-space factors multiplying the $^V\mathcal{M}^{(0)}_{KK0}$ matrix element. A similar argument can be used when comparing the relative magnitudes of the matrix elements in the NLO. The contribution of the NLO relative to that of the LO, is suppressed by the overall small phase-space factors, as discussed in [34, 44].

As seen in Table IV, the NMEs for ^{59}Fe have consistent values for the two interactions. In the case of ^{60}Fe, the magnitudes of the computed axial-vector matrix elements are found to be larger for the GXPF1A interaction than for the KB3G interaction, leading to strong differences in the shape factors. This difference can be traced back to the differences in the behavior of the cumulative sums of the vector and axial-vector matrix elements, exemplified by the vector matrix element $^V\mathcal{M}^{(0)}_{KK0}(1,1,1,1)$ and the axial-vector matrix element $^A\mathcal{M}^{(0)}_{KK1}(1,1,1,1)$ in Fig. 3. In this figure the cumulative sums of these matrix elements are plotted as functions of the contributing proton-neutron orbitals. As seen in the figure, for the

TABLE III: Calculated absolute values of the Gamow-Teller ($|\mathcal{M}_{\rm GT}|$) and Fermi ($|\mathcal{M}_{\rm F}|$) matrix elements of the allowed β^- decays from the ground-state ($3/2^-$) of ^{59}Fe to the first two excited $3/2^-$ states in ^{59}Co. The experimental Gamow-Teller matrix elements are obtained from the measured $\log ft$ values [50] by assuming the value $g_{\rm A} = 1.27$ for the axial coupling strength.

	$\|\mathcal{M}_{\rm GT}\|$			$\|\mathcal{M}_{\rm F}\|$	
	Expt.	KB3G	GXPF1A	KB3G	GXPF1A
$3/2^- \rightarrow 3/2^-_1$	0.0904	0.0696	0.1586	7.24×10^{-6}	1.0×10^{-5}
$3/2^- \rightarrow 3/2^-_2$	0.2064	0.0677	0.0345	3.49×10^{-6}	2.2×10^{-5}

TABLE IV: Leading-order (LO) and next-to-leading-order (NLO) nuclear matrix elements (NMEs) of the second-forbidden nonunique β^- decays of ^{59,60}Fe, computed using the KB3G and GXPF1A interactions. The CVC-constrained s-NMEs, ${}^{V}\mathcal{M}^{(0)}_{KK-11}$(CVC) (second line), are compared with the half-life fixed s-NMEs (for $g_{\rm A} = 0.80$), ${}^{V}\mathcal{M}^{(0)}_{KK-11}$(Half-life) (third line). The Coulomb-corrected NMEs are indicated by (k_e, m, n, ρ), when such elements exist. The blank spaces denote vanishing NMEs.

Transition	^{59}Fe$(3/2^-) \rightarrow {}^{59}Co(7/2^-)$		^{60}Fe$(0^+) \rightarrow {}^{60}Co(2^+)$	
NMEs	KB3G	GXPF1A	KB3G	GXPF1A
LO				
${}^{V}\mathcal{M}^{(0)}_{KK-11}$	0	0	0	0
${}^{V}\mathcal{M}^{(0)}_{KK-11}$(CVC)	0.2164	0.1921	0.2862	0.3055
${}^{V}\mathcal{M}^{(0)}_{KK-11}$(Half-life)	0.1037	0.0950	0.1143	0.0919
${}^{V}\mathcal{M}^{(0)}_{KK0}$	13.2021	11.7172	20.3265	21.6968
$(1,1,1,1)$	15.3084	13.6063	23.6439	25.2589
$(2,1,1,1)$	14.4779	12.8727	22.3782	23.9122
${}^{A}\mathcal{M}^{(0)}_{KK1}$	7.7745	7.7344	13.3677	19.7997
$(1,1,1,1)$	8.8039	8.7879	15.2409	22.8508
$(2,1,1,1)$	8.2773	8.2694	14.3539	21.5871
${}^{A}\mathcal{M}^{(0)}_{K+1K1}$	5.6712	4.5057	$--$	$--$
NLO				
${}^{V}\mathcal{M}^{(1)}_{KK-11}$	-0.1383	-0.1261	-0.1965	-0.2135
$(1,1,1,1)$	-0.1321	-0.1197	-0.1856	-0.1968
$(2,1,1,1)$	-0.1187	-0.1074	-0.1664	-0.1752
$(1,2,1,1)$	0.0242	0.0223	0.0351	0.0395
$(2,2,1,1)$	0.0169	0.0156	0.0245	0.0276
$(1,2,2,1)$	-0.1563	-0.1420	-0.2207	-0.2363
$(2,2,2,1)$	-0.1527	-0.1387	-0.2154	-0.2303
$(1,2,2,2)$	-0.1782	-0.1613	-0.2498	-0.2635
$(2,2,2,2)$	-0.1711	-0.1547	-0.2396	-0.2520
${}^{A}\mathcal{M}^{(1)}_{KK1}$	9.7384	9.5861	16.3829	23.3149
${}^{V}\mathcal{M}^{(0)}_{KK+11}$	9.6599	8.8069	13.8826	15.0793
$(1,1,1,1)$	11.0414	10.0325	15.7677	16.8896
$(2,1,1,1)$	10.4128	9.4538	14.8478	15.8523
${}^{V}\mathcal{M}^{(0)}_{K+1K+11}$	4.7566	4.3644	$--$	$--$
$(1,1,1,1)$	5.3167	4.9067	$--$	$--$
$(2,1,1,1)$	4.9860	4.6078	$--$	$--$
${}^{A}\mathcal{M}^{(0)}_{K+1K+11}$	2.2945	1.4936	$--$	$--$
$(1,1,1,1)$	2.8225	1.8565	$--$	$--$
$(2,1,1,1)$	2.7069	1.7847	$--$	$--$

vector matrix element there is a shift in the contributions of the proton-neutron orbital pairs from the very begin-

TABLE V: Values of the s-NME ${}^{V}\mathcal{M}^{(0)}_{KK-11}$ for the studied transitions in ^{59,60}Fe. For these values the calculations reproduce the measured half-life for each value of $g_{\rm A}$.

	${}^{59}\mathrm{Fe}(3/2^-) \to {}^{59}\mathrm{Co}(7/2^-)$		${}^{60}\mathrm{Fe}(0^+) \to {}^{60}\mathrm{Co}(2^+)$	
$g_{\rm A}$	KB3G	GXPF1A	KB3G	GXPF1A
0.80	0.10371	0.09499	0.11429	0.09187
0.90	0.09883	0.09009	0.10718	0.08093
1.00	0.09391	0.08515	0.10003	0.06987
1.10	0.08894	0.08017	0.09282	0.05869
1.20	0.08393	0.07515	0.08555	0.04739
1.27	0.08039	0.07161	0.08044	0.03941

ning such that these shifts conspire to produce a similar total vector matrix element for both interactions. For the axial-vector matrix elements this shift realizes only for the p-f proton-neutron orbital contributions. The difference between the shell model interactions stems from the contributions of p-orbital protons with neutrons not in the $f_{7/2}$ orbital. This difference in the cumulative behavior is driven by the differences in the values of the vector-type and axial-vector-type single-particle transition matrix elements ${}^{V/A}m^{(N)}_{KLS}(pn)$ in Eq. (6). Next we use these computed NMEs in order to evaluate the electron spectral shapes as functions of $g_{\rm A}$ for the studied transitions.

C. Electron spectral shapes and the effective value of $g_{\rm A}$

In the SSM, the shape of the β spectrum could be used to extract the effective values of the weak coupling constants by comparing the computed spectrum with the measured one for forbidden nonunique β decays. In order to facilitate this comparison with the potentially measured future spectrum-shape data, we present here the shapes of the electron spectra of the second-forbidden nonunique β^- decays of ^{59,60}Fe by varying the value of the axial-vector coupling $g_{\rm A}$ within a physically relevant interval. For the electron spectral shapes we have performed three sets of calculations in order to see the effects of the adopted values of the s-NME on the electron spectral shapes. In these calculations the s-NMEs are taken 0) to come from the bare interaction (thus having zero value), labeled in the figures with "interaction name;" or from the enhanced SSM procedures where the value of the s-NME comes i) from the CVC relation, labeled in the figures with "interaction name+CVC", or ii) from the fitting of the measured partial half-life, labeled in the figures with "interaction name+Half-life". The method i) makes the tacit assumption of an "ideal" calculation, in an infinite single-particle space with all two- and higher-body correlations included. Method ii) is more appropriate for the present situation where impulse approximation is assumed, together with severe restrictions in the single-particle space. Also, experimental data is best reproduced by using the method ii), so it can be seen as the most reliable in predicting the correlation between the spectral shape and the value of $g_{\rm A}$. Thus, from the point of view of the application of the SSM, the $g_{\rm A}$ sensitivity of the spectral shapes obtained by using the method ii) is the key issue. It is also to be noted that all the transitions have been observed experimentally but the electron spectra are not yet available. For the β^--decay transition in ^{59}Fe the measured branching is less than 1% and for the transition in ^{60}Fe we have a 100% branching.

The computed shape factors (left panels) and electron spectra (right panels), corresponding to the decay transitions in ^{59,60}Fe, are shown in Figs. 4–7 for the range $g_{\rm A} = 0.80 - 1.27$ of the axial coupling. In these figures are presented the shape factor of Eq. (5) and the electron spectra corresponding to the integrand of Eq. (4) as functions of the electron kinetic energy, computed separately for the KB3G and GXPF1A interactions. We have chosen to normalize the area under each curve to unity in order to facilitate easy comparison with the potential future data.

The electron spectra of ^{59}Fe are shown in the Figs. 4 and 5 for the KB3G and GXPF1A interactions, respectively. For the bare interaction (our method 0)), the computed electron spectral shapes strongly depend on the value of $g_{\rm A}$. After constraining the value of the s-NME by the CVC relation (our enhanced method i)), the electron spectral shapes become almost insensitive to $g_{\rm A}$, while for the half-life-determined s-NMEs (our enhanced method ii)) the spectrals shapes are moderately sensitive for both interactions. As seen in the figures, the spectra for each individual computation method show similar behaviour for both interactions. In particular for the method ii), of interest for the comparison with the potential future data, the electron spectral shapes computed with the two interactions are consistent with each other. In this case, the differences of the spectra for different $g_{\rm A}$ values are more pronounced for the low-energy part of the spectra, below 0.5 MeV of electron energy, or for the middle part,

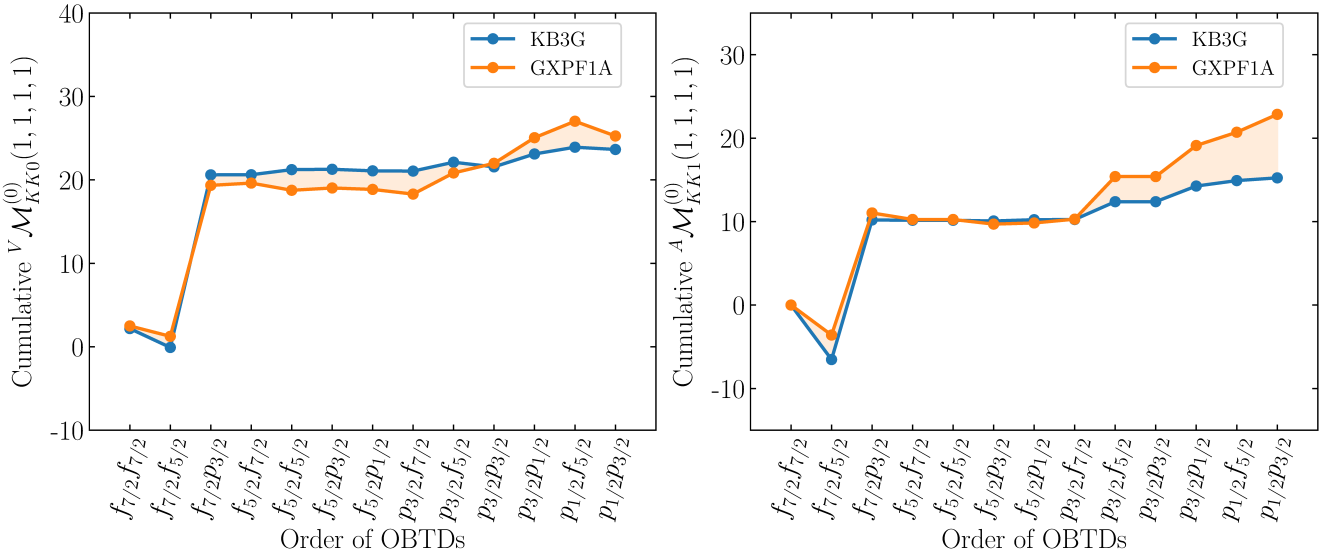

FIG. 3: Cumulative sum of the vector matrix element $^{V}\mathcal{M}^{(0)}_{KK0}(1,1,1,1)$ (left panel) and the axial-vector matrix element $^{A}\mathcal{M}^{(0)}_{KK1}(1,1,1,1)$ (right panel) for the decay of ^{60}Fe. The horizontal axis lists the contributing proton-neutron orbital pairs.

between 0.7 MeV and 1.2 MeV of electron energy. This low-energy part is the harder part for the experiments to measure due to growing backgrounds which mask the exact experimental shape. In the middle electron energy region above 0.7 MeV the differences between the spectra are easier to resolve experimentally owing to a smaller background contribution. It is our hope that the energy threshold of a dedicated beta-decay experiment could go well below 0.5 MeV, as was the case for the ^{113}Cd experiments performed by Belli *et al.* [35] and by the COBRA collaboration [51]. In the present case a potential additional difficulty may be the small branching ratio, 0.18(4)%, of the ground-state transition.

The electron spectra of the β^--decay transition of ^{60}Fe have previously been computed by Kostensalo *et al.* in Ref. [37]. For this calculation, they have used the old Horie-Ogawa interaction, constrained to orbitals $\pi 0f_{7/2}$, $\nu 1p_{3/2}$, $\nu 0f_{5/2}$ and $\nu 1p_{1/2}$. They have performed the calculations for the electron spectra by using the pure shell-model-predicted matrix elements, without the CVC correction. From this interaction, the shape of electron spectra turns out to be independent of $g_{\rm A}$. In our case, we have used the complete $0\hbar\omega$ shell-model calculations in a full fp model space with the well-established KB3G and GXPF1A interactions, and also constrained the value of the s-NME using the enhanced SSM procedures i) and ii). Our predicted shape factors and electron spectra for the β transition of ^{60}Fe, corresponding to the KB3G and GXPF1A interactions, are shown in the Figs. 6 and 7, respectively. The computed electron spectra from the bare interaction are found, again, to strongly depend on the value of $g_{\rm A}$. Interestingly enough, the predicted shape factors and electron spectra for the two interactions are found to behave differently as functions of $g_{\rm A}$. This contradicting behavior is resolved in the enhanced SSM procedures i) and ii). After fixing the value of the s-NME, the $g_{\rm A}$ dependence of the electron spectral shapes is qualitatively similar for both used interactions. In the case of the method ii), relevant for the experimental comparison, the spectral shapes are found to be moderately dependent on $g_{\rm A}$. The sensitivity to $g_{\rm A}$ is most pronounced for the low electron energies, below some 0.05 MeV. Some $g_{\rm A}$ dependence is found also for the middle region of electron energies.

In Fig. 8, in the case of the ^{60}Fe decay, we present the relative NLO corrections to partial half-life as functions of the value of $g_{\rm A}$ for calculations using the bare interactions, without any s-NME adjustments. As seen in this figure, the effects of the NLO corrections to the half-life are strongly dependent on the value of $g_{\rm A}$. Adding the NLO corrections leads at most to an about 18% correction to the partial half-life, corresponding to the values of $g_{\rm A} = 1.22$ and $g_{\rm A} = 0.88$ for the KB3G and GXPF1A interactions, respectively. The partial half-life increases for $g_{\rm A}$ values below these values and decreases fast within a short interval after that. The NLO corrections affect also the electron spectral shapes as seen in Fig. 9, where the spectra are plotted at the above-mentioned $g_{\rm A}$ values which give the maximum effects on the half-life in the bare-interaction calculations. We can see from the figure that the effects of the NLO corrections are most significant at the low electron energies for both the KB3G and GXPF1A interactions. Interestingly enough, these cases are the extreme ones, and performing the s-NME adjustments according to the methods i) and ii) dampens the NLO effects considerably, and in these cases the partial half-lives and electron spectra collect negligible contributions from the NLO corrections to the β-decay shape function.

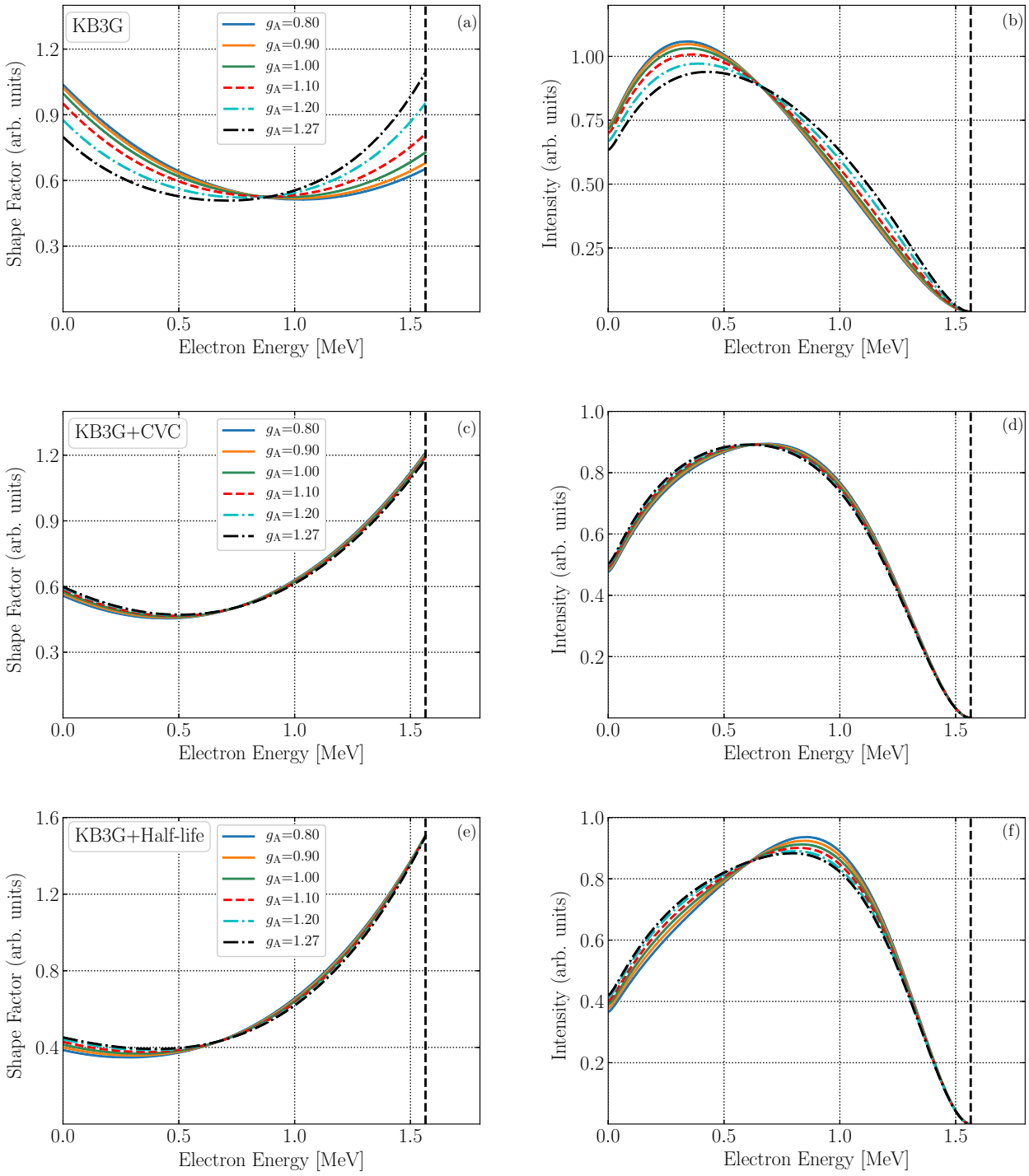

FIG. 4: The KB3G-computed shape factors (left panels) and electron spectra (right panels) as functions of the electron kinetic energy for the second-forbidden nonunique β^- transition ^{59}Fe$(3/2^-) \rightarrow {}^{59}Co(7/2^-)$. The dashed vertical lines represent the end-point energy of the transition and the area under each curve is normalized to unity. The top panels refer to the results of the original interaction (zero value of the s-NME), the figures of the middle panel use the CVC-constrained value of the s-NME and the figures of the bottom panel are obtained by using the fitted values of the s-NME.

D. Decomposition of the integrated shape function

We have decomposed the integrated shape function to see the individual effects of the vector $\tilde{C}_{\rm V}$, axial-vector $\tilde{C}_{\rm A}$, and mixed vector-axial-vector $\tilde{C}_{\rm VA}$ components [see Eq. (8)]. The integrated shape function $\tilde{C}$ and its de-

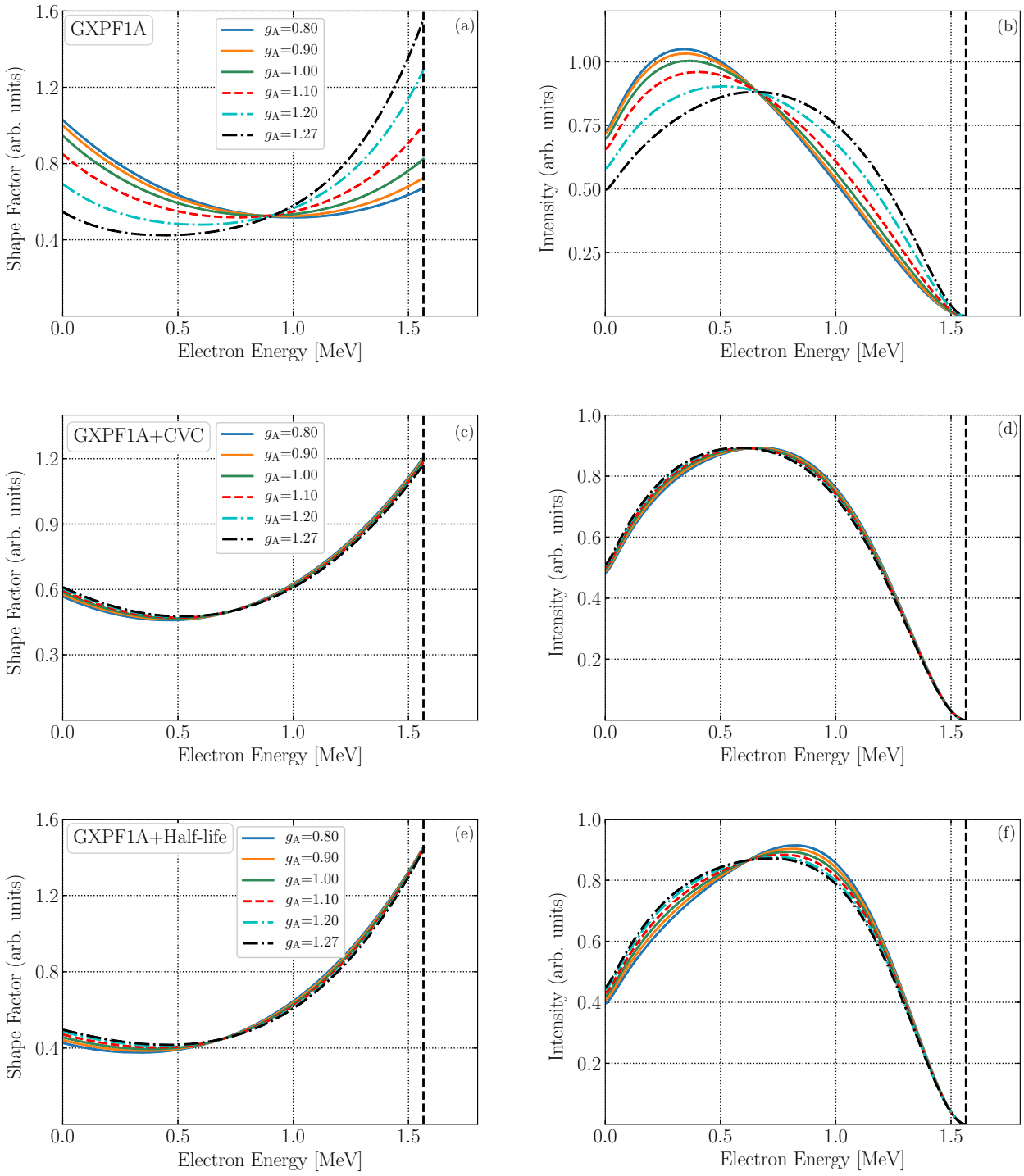

FIG. 5: The same as in Fig. 4 for the GXPF1A interaction.

composed components for the studied decay transitions, computed with the KB3G and GXPF1A interactions, are presented in Table VI for $g_V = g_A = 1.00$. For both interactions and studied transitions, the signs of the vector $\tilde{C}_V$ and axial-vector $\tilde{C}_A$ components are positive for all approaches of calculation.

In the case of ^{59}Fe, the mixed vector-axial-vector component is negative for the bare interaction calculations and positive for methods i) and ii). For both interactions, the vector contribution is larger than the axial-vector contribution in the calculations using the bare interaction and method i), while in the case of method ii) the

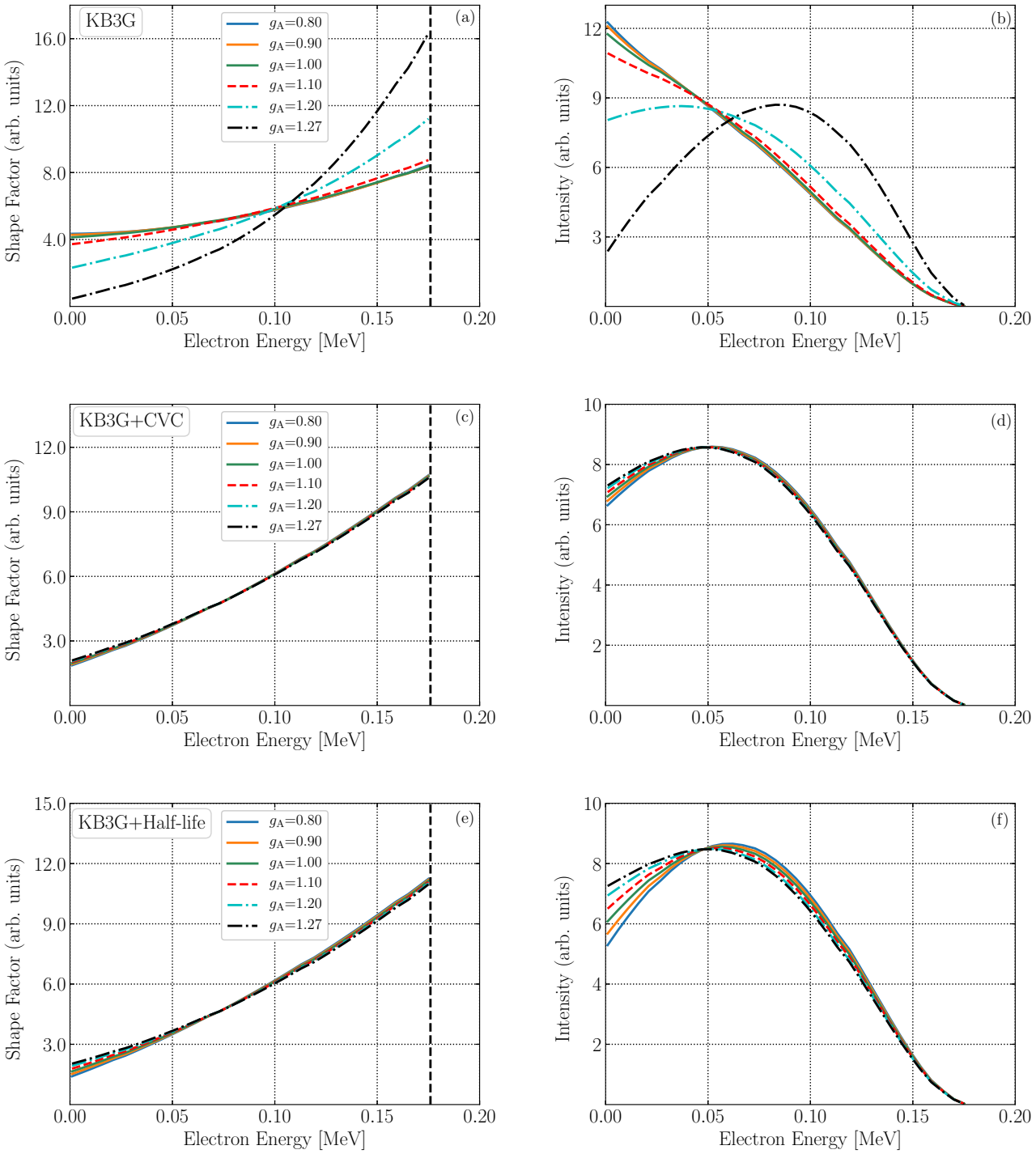

FIG. 6: The same as in Fig. 4 for KB3G interaction and for the β-decay transition $^{60}\mathrm{Fe}(0^+) \rightarrow {}^{60}\mathrm{Co}(2^+)$.

axial part dominates. For the bare interaction calculation of ^{59}Fe, the $\tilde{C}_{\mathrm{A}}$ component is about 36% (KB3G) and 45% (GXPF1A) of the vector component and the mixed component $\tilde{C}_{\mathrm{VA}}$ is slightly less than the sum of $\tilde{C}_{\mathrm{V}}$ and $\tilde{C}_{\mathrm{A}}$, and negative for both interactions. After constraining the s-NME, the decomposition for ^{59}Fe is surprisingly similar for both interactions. In method i), for both interactions, the axial-vector component contributes little to the total integrated shape function, while in the method ii) the contribution of the vector component is very small for both interactions. In the case of ^{60}Fe, for both interactions, the mixed component is negative for the bare-

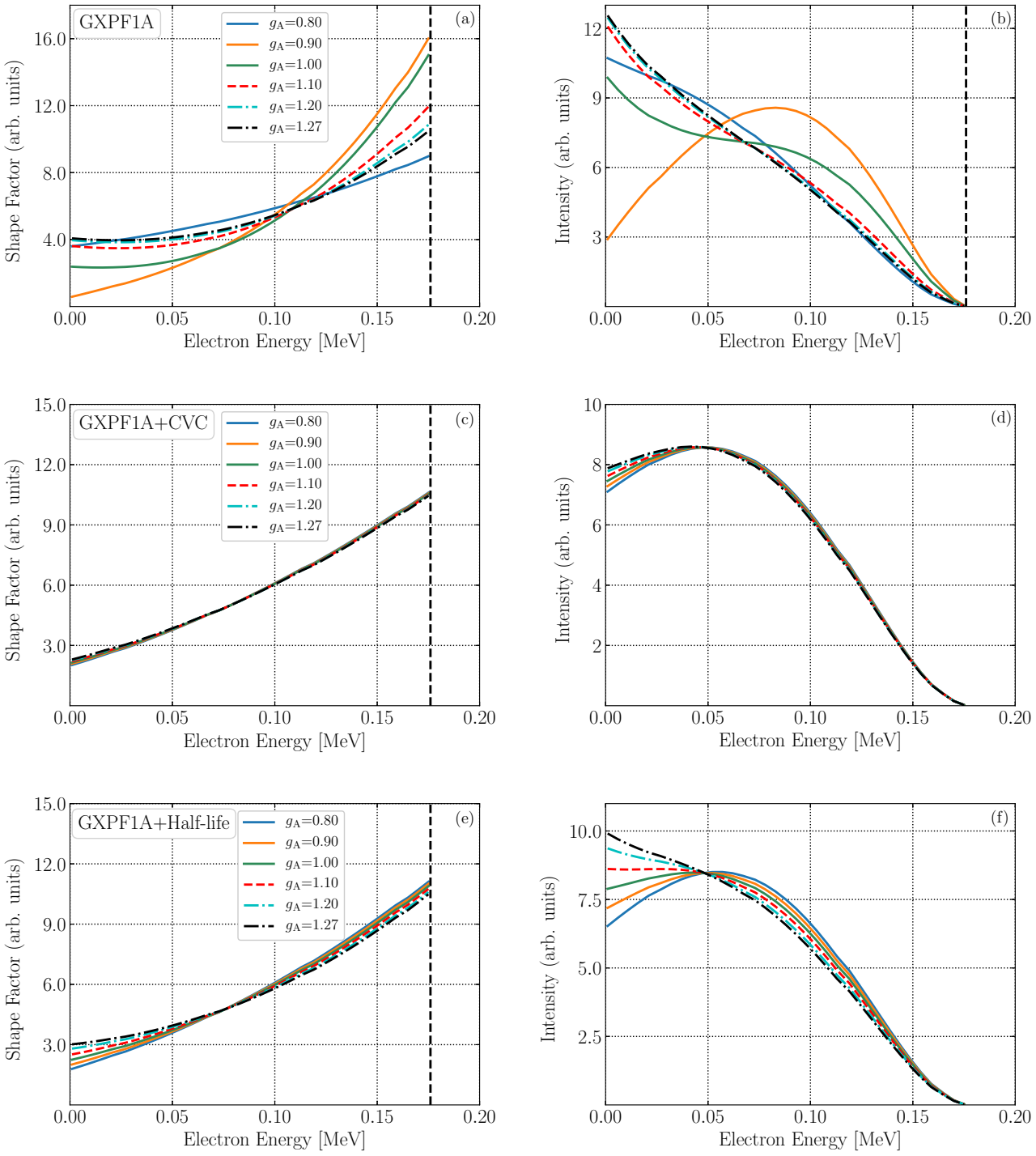

FIG. 7: The same as in Fig. 4 for GXPF1A interaction and for the β-decay transition $^{60}\mathrm{Fe}(0^+) \rightarrow {}^{60}\mathrm{Co}(2^+)$.

interaction and method ii) calculations, while positive for the method i). In the bare-interaction calculations, the vector and axial-vector components are roughly equally strong, but for the method i) the vector part dominates and for the method ii) the axial part dominates. One also notices that for the bare-interaction calculations the mixed component $\tilde{C}_{\mathrm{VA}}$ is negative and its magnitude is almost the sum of the $\tilde{C}_{\mathrm{V}}$ and $\tilde{C}_{\mathrm{A}}$ components. After constraining the value of s-NME, this degeneracy is lifted, in particular in the case of the method ii).

TABLE VI: Decomposition of the dimensionless integrated shape function into vector $\tilde{C}_{\rm V}$, axial-vector $\tilde{C}_{\rm A}$, and mixed vector-axial-vector $\tilde{C}_{\rm VA}$ components for $g_{\rm V} = g_{\rm A} = 1.00$.

	^{59}Fe($3/2^-$) $\rightarrow$ ^{59}Co($7/2^-$)			
	$\tilde{C}_{\rm V}$	$\tilde{C}_{\rm A}$	$\tilde{C}_{\rm VA}$	$\tilde{C}$
KB3G	5.829×10^{-6}	2.111×10^{-6}	-6.853×10^{-6}	1.088×10^{-6}
GXPF1A	4.602×10^{-6}	2.092×10^{-6}	-6.079×10^{-6}	6.148×10^{-7}
KB3G+CVC	1.410×10^{-5}	2.111×10^{-6}	9.795×10^{-6}	2.600×10^{-5}
GXPF1A+CVC	1.110×10^{-5}	2.092×10^{-6}	8.677×10^{-6}	2.187×10^{-5}
KB3G+Half-life	4.623×10^{-7}	2.111×10^{-6}	3.716×10^{-7}	2.945×10^{-6}
GXPF1A+Half-life	3.912×10^{-7}	2.092×10^{-6}	4.615×10^{-7}	2.945×10^{-6}
	^{60}Fe(0^+) $\rightarrow$ ^{60}Co(2^+)			
	$\tilde{C}_{\rm V}$	$\tilde{C}_{\rm A}$	$\tilde{C}_{\rm VA}$	$\tilde{C}$
KB3G	1.199×10^{-10}	7.123×10^{-11}	-1.845×10^{-10}	6.561×10^{-12}
GXPF1A	1.368×10^{-10}	1.606×10^{-10}	-2.961×10^{-10}	1.381×10^{-12}
KB3G+CVC	4.615×10^{-10}	7.123×10^{-11}	3.339×10^{-10}	8.666×10^{-10}
GXPF1A+CVC	5.253×10^{-10}	1.606×10^{-10}	5.352×10^{-10}	1.221×10^{-9}
KB3G+Half-life	8.225×10^{-12}	7.123×10^{-11}	-3.349×10^{-12}	7.611×10^{-11}
GXPF1A+Half-life	2.144×10^{-11}	1.606×10^{-10}	-1.060×10^{-10}	7.611×10^{-11}

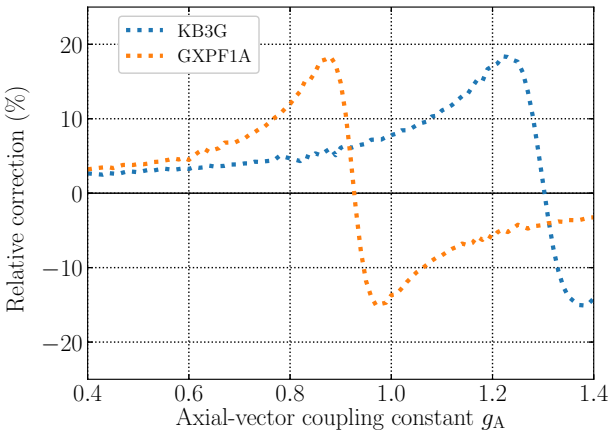

FIG. 8: Relative correction to the partial half-life for the β^--decay of ^{60}Fe stemming from the NLO corrections to the shape factor (i.e., with s-NME= 0). The relative correction is presented as a function of the value of the axial-vector coupling $g_{\rm A}$.

To give a rough idea of the needed experimental resolution in the determination of the effective value of $g_{\rm A}$ from the beta spectra computed using the method ii), we have picked as an example the decay of ^{59}Fe, computed with the KB3G interaction. The corresponding comparison is shown in Fig. 10, where we have picked the energy region $0.2-0.4$ MeV of the beta spectrum of Fig. 4-(f), since in this interval the sensitivity of the spectrum to $g_{\rm A}$ is the strongest. In Fig. 10 we show the change in the spectral shape in percents when changing $g_{\rm A}$ by 0.1, 0.2, and 0.3 units within the interval $g_A = 0.8-1.27$. One can see that when one wants one-unit resolution in the value of $g_{\rm A}$ the corresponding change in he beta spectrum is of the order of $1-3\%$. For a two-unit or a three-unit resolution the corresponding spectral changes are in the ballpark of $4-6\%$ and $6-8\%$, respectively. Similar percentual sensitivities of the beta spectra to the changes in the value of $g_{\rm A}$ are also recorded for the other cases treated by using method ii).

E. Critical assessment of the present status of calculations

We have presented in the previous sections the results of our search for $g_{\rm A}$-sensitive electron spectral shapes in the fp shell-model valence space. We have found two potential candidate transitions, ^{59}Fe($3/2^-$) $\rightarrow$ ^{59}Co($7/2^-$) and ^{59}Fe($3/2^-$) $\rightarrow$ ^{59}Co($7/2^-$), with some sensitivity in their spectral shapes to the variation in the value of $g_{\rm A}$. However, in order these cases to be useful for possible future measurements, it is may be necessary to improve the present calculations and access the systematic errors of

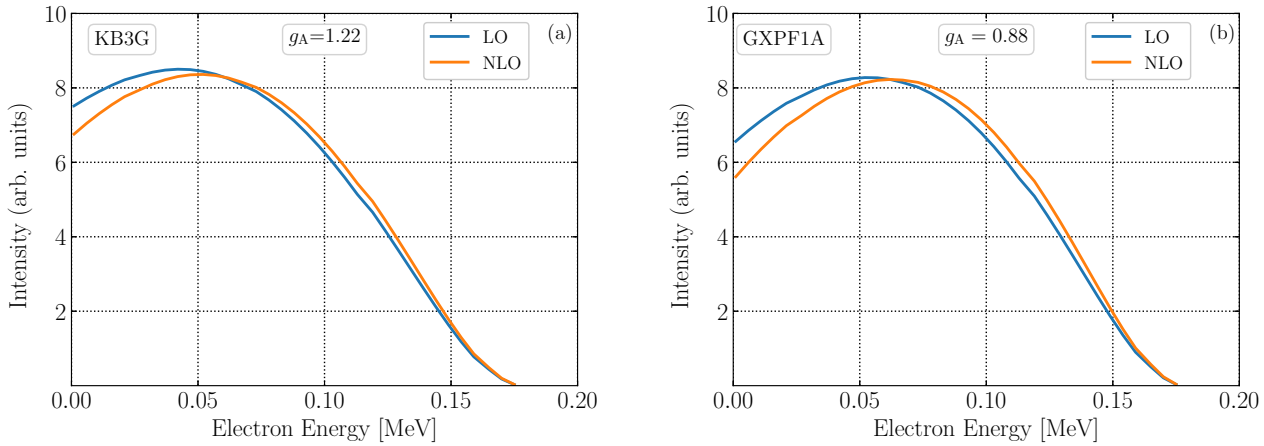

FIG. 9: Electron spectral shapes for the decay of ^{60}Fe, computed using the bare KB3G (left panel) and GXPF1A (right panel) interactions (i.e., with s-NME= 0). The indicated g_A values of each panel correpond to those in Fig. 8 for which the maximal NLO corrections to the partial half-life are achieved.

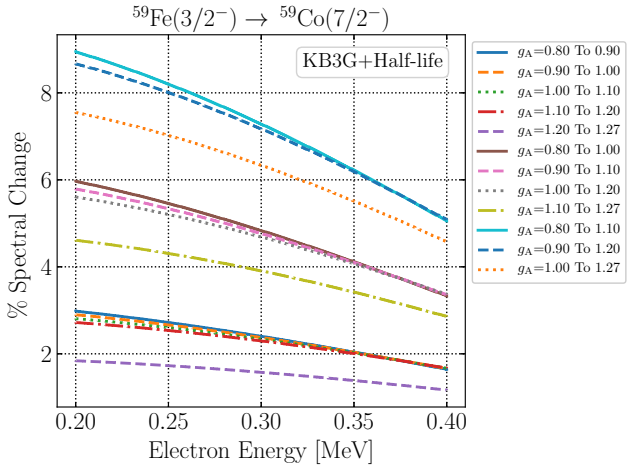

FIG. 10: Percentual changes in the beta spectrum shape of Fig. 4-(f), computed by using the interaction KB3G, in the energy region 0.2 − 0.4 MeV. The spectral changes correspond to changes in the value of g_A by 0.1, 0.2, and 0.3 units within the interval $g_A = 0.8 - 1.27$.

them. The critical aspects of the present calculations relate to the determination of the values of the large vector NME $^V\mathcal{M}^{(0)}_{220}$ and the s-NME $^V\mathcal{M}^{(0)}_{211}$. First, the present calculations use only the fp valence space leaving out possible particle-hole contributions from the adjacent shells, like the gds shell above. These excitations could alter the value of the large NME, as also the values of the other NMEs, including the value of the s-NME, involved in the calculations. Second, the present way of determining the value of the s-NME through the CVC relation from the large NME [method i)] has uncontrolled uncertainties in it related to the fact that the present calculations are not "ideal", and subject to a severe truncation in the valence single-particle space. The method ii) uses the s-NME as a fit parameter, thus compensating the error in the present half-life calculation stemming from the limited valence space. In both methods, then many uncertainties can be present and extension of the presently used valence space is in order in possible future calculations. In this way one can at least have an estimate of the uncertainties related to the spectral-shape calculations.

A further complication in the present calculations are the different ways the many operators involved in the present calculations can be renormalized by the limited valence space and/or the true renormalization of the weak axial current. The renormalization can be different for the operators of axial and vector type, further complicating the interpretation of the present, small model-space, calculations. In this respect the forbidden unique transitions offer a much simpler approach since they are driven by a single axial NME and direct comparison of the computed and measured half-lives is in a position to make the determination of a "quenching factor" a rather straighforward procedure. Again, this quenching factor includes both the valence-space renormalization and the renormalization of the weak axial current. However, it could be imagined that in reasonably robust nuclear-model calculations in the future the two methods, SSM and the unique-forbidden scheme, could offer complementary information of the renormalization of the axial current and valence-space effects. These robust calculations should take into account, in addition to the presently included NLO corrections, also the effects of the two-body currents, as discussed recently in [31]. The effect of these currents could be expectred to play a role of at least of similar magnitude as the NLO corrections to the nonunique forbidden beta decays.

IV. CONCLUSIONS

In this work we have performed a search in the fp shell for possible forbidden nonunique beta transitions for which the associated beta spectrum shape depends notably on the value of the axial coupling $g_{\rm A}$, thus allowing the use of the spectrum-shape method in this context. We have found two candidate transitions, and we have performed a full $0\hbar\omega$ calculation of the shape factors and electron spectra for the second-forbidden nonunique β^--decay transitions ^{59}Fe$(3/2^-) \rightarrow {}^{59}Co(7/2^-)$ and ^{60}Fe$(0^+) \rightarrow {}^{60}Co(2^+)$ in the full fp single-particle space using the well-established effective shell-model interactions KB3G and GXPF1A. We include also the next-to-leading-order corrections to the β-decay shape factor.

To test the predictive power of the adopted interactions, we have calculated the low-lying energy spectra of the parent and daughter nuclei participating in the studied β^- transitions and compared the results with the available data. The low-lying energy spectra agree reasonably with the experimental data and only for ^{60}Co we are unable to obtain the correct ground state. Also the spectroscopic properties are reasonably well predicted by these effective interactions. The obtained wave functions have been used for further calculations of the β-decay rates.

In the present work, we have enhanced the original SSM by constraining the value of the small vector NME (s-NME) ${}^V\mathcal{M}^{(0)}_{KK-11}$ in two different ways: either by i) directly using a CVC relation, or ii) reproducing the experimental partial half-life by tuning the value of this matrix element. In the method ii), we have constraint the s-NME for each $g_{\rm A}$ separately. The computed values of the s-NME are found to deviate by a factor of 2-3 between the two approaches, depending on the used interaction. The evolution of the shape factors and electron spectra for the two second-forbidden nonunique β^--decay transitions was studied within the interval of $g_{\rm A} = 0.80 - 1.27$ using the two shell-model interactions. We found that the computed shape factors and electron spectra are sensitive to the value of the s-NME ${}^V\mathcal{M}^{(0)}_{KK-11}$. The enhancement method ii) is to be considered as the preferred one over i) since it can be used under the assumption of the impulse approximation and for restricted shell-model single-particle spaces. It also makes possible to reproduce the partial half-lives of the studied β-decay transitions in the calculations. At the end of the results section (Sec. III E) we have also taken a critical look at the deficiencies and the resulting inaccuracies of the present nuclear-model calculations.

In the case of the method ii), the shapes of the electron spectra depend somewhat on the value of $g_{\rm A}$ for both studied transitions, thus opening up the possibility to use this revised SSM to access the effective value of $g_{\rm A}$ in these cases. For ^{60}Fe the decay transition has a branching ratio of 100%, making it a perfect candidate for future spectral-shape measurements and a subsequent application of the enhanced SSM. In order to see the origin of these variations in the electron spectral shapes we have decomposed the total integrated shape function $\tilde{C}$ into its vector $\tilde{C}_{\rm V}$, axial-vector $\tilde{C}_{\rm A}$, and mixed vector-axial-vector $\tilde{C}_{\rm VA}$ components. The relative sizes and signs of these components lead to sensitivity or non-sensitivity of the spectral shapes to the value of $g_{\rm A}$. We hope that in the future we can improve the characterization of the inaccuracies related to the used nuclear models in the context of the SSM. We nevertheless hope that our theoretical work strongly encourages future measurements of electron spectral shapes.

Acknowledgments

A. K. would like to thank the Ministry of Human Resource Development (MHRD), Government of India, for the financial support for his Ph.D. thesis work. P.C.S. acknowledges a research grant from SERB (India), CRG/2019/000556. J. S. has been partially supported by the academy of Finland under the academy project no. 318043.

[1] K. Zuber, "*Neutrino Physics*", (Institue of Physics Publishing Ltd., London 2004).
[2] E. D. Commins "*Weak Interactions*" (McGraw-Hill, New York, 2007).
[3] J. Suhonen and O. Civitarese, "Weak-interaction and nuclear-structure aspects of nuclear double beta decay", Phys. Rep. **300**, 123 (1998).
[4] J. Maalampi and J. Suhonen, "Neutrinoless Double β^+/EC Decays", Adv. High Energy Phys. **2013**, 505874 (2013).
[5] J. Suhonen, "Value of the axial-vector coupling strength in β and $\beta\beta$ decays: a review", Frontier in Physics **5**, 55 (2017).
[6] H. Ejiri, J. Suhonen, and K. Zuber, "Neutrino-nuclear responses for astro-neutrinos, single beta decays and double beta decays ", Phys. Rep. **797**, 1 (2019).
[7] H. Ejiri, N. Soukouti, and J. Suhonen, "Spin-dipole nuclear matrix elements for double beta decays and astro-neutrinos", Phys. Lett. B **729**, 27 (2014).
[8] H. Ejiri and J. Suhonen, "GT neutrino-nuclear responses for double beta decays and astro neutrinos", J. Phys. G: Nucl. Part. Phys. **42**, 055201 (2015).
[9] J. Suhonen and O. Civitarese, "Probing the quenching of g_A by single and double beta decays", Phys. Lett. B **725**, 153 (2013).
[10] J. Suhonen and O. Civitarese, "Single and double beta decays in the $A = 100$, $A = 116$ and $A = 128$ triplets of isobars", Nucl. Phys. A **924**, 1 (2014).
[11] A. Faessler, G. L. Fogli, E. Lisi, V. Rodin, A. M. Rotunno, and F. Šimkovic, "Overconstrained estimates

of neutrinoless double beta decay within the QRPA", J. Phys. G: Nucl. Part. Phys. **35**, 075104 (2008)
[12] D. S. Delion and J. Suhonen, "Effective axial-vector strength and β-decay systematics", Eur. Phys. Lett. **107**, 52001 (2014).
[13] P. Pirinen and J. Suhonen, "Systematic approach to β and $2\nu\beta\beta$ decays of mass $A = 100 - 136$ nuclei", Phys. Rev. C **91**, 054309 (2015).
[14] F. F. Deppisch and J. Suhonen, "Statistical analysis of β decays and the effective value of g_A in the proton-neutron quasiparticle random-phase approximation framework", Phys. Rev. C **94**, 055501 (2016).
[15] B. H. Wildenthal, M. S. Curtin, and B. A. Brown, "Predicted features of the beta decay of neutron-rich sd-shell nuclei", Phys. Rev C **28**, 1343 (1983).
[16] G. Martínez-Pinedo, A. Poves, E. Caurier, and A. P. Zuker, "Effective g_A in the pf shell", Phys. Rev. C. **53**, R2602 (1996).
[17] E. Caurier, F. Nowacki, and A. Poves, "Shell Model description of the $\beta\beta$ decay ^{136}Xe", Phys. Lett. B **711**, 62 (2012).
[18] V. Kumar, P.C. Srivastava, and H. Li, "Nuclear β^--decay half-lives for fp and fpg shell nuclei" Jour. Phys. G: Nucl. and Part. Phys. **43**, 105104 (2016).
[19] V. Kumar and P.C. Srivastava, "Shell model description of Gamow-Teller strengths in pf-shell nuclei" Eur. Phys. J. A **52**, 181 (2016).
[20] A. Saxena, P.C. Srivastava and T. Suzuki, "Ab initio calculations of Gamow-Teller strengths in the sd shell", Phys. Rev. C **97**, 024310 (2018).
[21] A. Kumar, P.C. Srivastava and T. Suzuki, "Shell model results for nuclear β^--decay properties of sd-shell nuclei", Prog. Theo. Expt. Phys. **2020**, 033D01 (2020).
[22] J. Kostensalo and J. Suhonen, "Consistent large-scale shell-model analysis of the two-neutrino $\beta\beta$ and single β branchings in ^{48}Ca and ^{96}Zr", Phys. Lett. B **802**, 135192 (2020).
[23] J. Barea, J. Kotila, and F. Iachello, "$0\nu\beta\beta$ and $2\nu\beta\beta$ nuclear matrix elements in the interacting boson model with isospin restoration", Phys. Rev. C **91**, 034304 (2015).
[24] J. Barea, J. Kotila, and F. Iachello, "Nuclear matrix elements for double-β decay", Phys. Rev. C **87**, 014315 (2015).
[25] N. Yoshida and F. Iachello, "Two-neutrino double-β decay in the interacting boson-fermion model", Prog. Theo. Expt. Phys. **2013**, 043D01 (2013).
[26] J. Suhonen and J. Kostensalo, "Double β decay and axial strength", Frontier in Physics **7**, 29 (2019).
[27] E. K. Warburton, "First-forbidden β decay in the lead region and mesonic enhancement of the weak axial curren", Phys. Rev. C **44**, 233 (1991).
[28] J. Kostensalo and J. Suhonen, "Mesonic enhancement of the weak axial charge and its effect on the half-lives and spectral shapes of first-forbidden $J^+ \leftrightarrow J^-$ decay", Phys. Lett. B **781**, 480 (2018).
[29] S. Pastore, A. Baroni, J. Carlson, S. Gandolfi, S. C. Pieper, R. Schiavilla, and R. B. Wiringa,"Quantum Monte Carlo calculations of weak transitions in $A = 6 - 10$ nuclei", Phys. Rev. C **97**, 022501(R) (2018).
[30] G. B. King, L. Andreoli, S. Pastore, M. Piarulli, R. Schiavilla, R. B. Wiringa, J. Carlson, and S. Gandolfi, "Chiral effective field theory calculations of weak transitions in light nuclei", Phys. Rev. C **102**, 025501 (2020).
[31] P. Gysbers, G. Hagen, J. D. Holt, G. R. Jansen, T. D. Morris, P. Navrátil, T. Papenbrock, S. Quaglioni, A. Schwenk, S. R. Stroberg and K. A. Wendt, "Discrepancy between experimental and theoretical β-decay rates resolved from first principles", Nat. Phys. **15**, 428 (2019).
[32] J. Engel and J. Menéndez, "Status and future of nuclear matrix elements for neutrinoless double-beta decay: a review", Rep. Prog. Phys. **80**, 046301 (2017).
[33] M. Haaranen, P. C. Srivastava, and J. Suhonen "Forbidden nonunique β decays and effective values of weak coupling constants", Phys. Rev. C **93** 034308 (2016).
[34] M. Haaranen, J. Kotila, and J. Suhonen, "Spectrum-shape method and the next -to-leading-order terms of the β-decay shape factor", Phys. Rev. C **95** 024327 (2017).
[35] P. Belli, R. Bernabei, N. Bukilic, F. Cappella, R. Cerulli, C. J. Dai, F. A. Danevich, J. R. de Laeter, A. Incicchitti, V. V. Kobychev, S. S. Nagorny, S. Nisi, F. Nozzoli, D. V. Poda, D. Prosperi, V. I. Tretyak, and S. S. Yurchenko, "Investigation of β decay of ^{113}Cd", Phys. Rev. C **76**, 064603 (2007).
[36] J. Kostensalo, M. Haaranen, and Jouni Suhonen, "Electron spectra in forbidden β decays and the quenching of the weak axial-vector coupling constant g_A", Phys. Rev. C **95**, 044313 (2017).
[37] J. Kostensalo and J. Suhonen, "g_A-driven shapes of electron spectra of forbidden β decays in the nuclear shell model", Phys. Rev. C **96**, 024317 (2017).
[38] A. Kumar, P. C. Srivastava, J. Kostensalo and J. Suhonen, "Second-forbidden nonunique β^- decays of ^{24}Na and ^{36}Cl assessed by the nuclear shell model", Phys. Rev. C. **101**, 064304 (2020).
[39] O. S. Kirsebom et. al., "Measurement of the $2^+ \rightarrow 0^+$ ground-state transition in the β decay of ^{20}F", Phys. Rev. C. **100**, 065805 (2019).
[40] O. S. Kirsebom et. al., "Discovery of an Exceptionally Strong β-Decay Transition of ^{20}F and Implications for the Fate of Intermediate-Mass Stars", Phys. Rev. Lett. **123**, 262701 (2019).
[41] M. Honma, T. Otsuka, B. A. Brown, and T. Mizusaki, "New effective interaction for pf-shell nuclei and its implications for the stability of the $N = Z = 28$ closed core", Phys. Rev. C **69** 034335 (2004).
[42] M. Honma, T. Otsuka, B. A. Brown, and T. Mizusaki, "Shell-model description of neutron-rich pf-shell nuclei with a new effective interaction GXPF1", Eur. Phys. J. A **25** 499 (2005).
[43] A. Poves, J. Sánchez-Solano, E. Caurier, and F. Nowacki, "Shell model study of the isobaric chains A = 50, A = 51 and A = 52", Nucl. Phys. A **694** 157 (2001).
[44] H. Behrens and W. Bühring, *Electron Radial Wave Functions and Nuclear Beta-Decay* (Clarendon Press, 1982).
[45] H. F. Schopper, *Weak Interaction and Nuclear Beta Decay* (North-Holland, Amsterdam, 1966).
[46] M. T. Mustonen, M. Aunola, and J. Suhonen, "Theoretical description of the fourth-forbidden non-unique β decays of ^{113}Cd and ^{115}In", Phys. Rev. C **73** 054301 (2006); Erratum Phys. Rev. C **76** 019901 (2007)
[47] J. Suhonen, *From Nucleons to Nucleus: Concept of Microscopic Nuclear Theory*, (Springer, Berlin 2007).
[48] C. Patrignani and Particle Data Group, "Review of Particle Physics", Chinese Phys. C **40**, 100001 (2016).
[49] B. A. Brown and W. D. M. Rae, "The Shell-Model Code NuShellX@MSU", Nucl. Data Sheets **120**, 115 (2014).
[50] NNDC, https://www.nndc.bnl.gov/ensdf/.

[51] L. Bodenstein-Dresler *et al.* (COBRA Collaboration), "Quenching of g_A deduced from the β-spectrum shape of ^{113}Cd measured with the COBRA experiment", Phys. Lett. B **800**, 135092 (2020).